*Original Research Article*

International journal of spray and combustion dynamics

International Journal of Spray and Combustion Dynamics
0(0) 1–14

DOI: 10.1177/1756827717695282
journals.sagepub.com/home/scd

SAGE

# Passive instability control by a heat exchanger in a combustor with nonuniform temperature

**Aswathy Surendran and Maria A Heckl**

**Abstract**

Thermoacoustic instabilities, caused by the feedback between unsteady heat release and acoustic pressure perturbations, are characterised by large-amplitude pressure oscillations. These oscillations, if uncontrolled, pose a threat to the integrity of combustion systems. One strategy to mitigate them is by installing cavity-backed perforated plates with bias flow into the combustion chamber. In this study, we consider a generic combustor configuration: a one-dimentional tube (with open and/or closed ends) containing a compact heat source and a heat exchanger tube row. The idea is to use the heat exchanger tube row as a device (analogously to a cavity-backed perforated plate) to manipulate the downstream end condition. We simulate the row of heat exchanger tubes by a slit-plate with bias flow. We derive the characteristic equation for the complex eigenfrequencies of this set-up. From the growth rates (imaginary parts of the eigenfrequencies), we construct stability maps for various system parameter combinations. The results, obtained for the first two modes of the system, show that by varying the cavity length or the bias flow velocity through the slits, we can stabilise a previously unstable combustion system.

**Keywords**

Thermoacoustic instabilities, control of instability, stability analysis, heat exchangers, orifice plates

Date received: 30 September 2016; accepted: 24 January 2017

## 1 Introduction

When a heat source like a flame or a heated gauze is placed within an acoustic resonator, there may be an interaction between the heat release fluctuations and the acoustic pressure fluctuations, which forms a positive feedback loop leading to high-amplitude oscillations. This effect has been observed in combustion systems and is known as thermoacoustic instability. If uncontrolled, high-pressure loads occur, leading to excessive vibrations of mechanical parts, and in extreme cases, to catastrophic hardware damage.[1] It is therefore important to develop mitigation strategies to prevent these instabilities.

Combustion systems that are prone to thermoacoustic instabilities are gas turbine engines, rocket motors, afterburners, furnaces and domestic heaters. There is a large variety of designs. Some of them include heat exchangers, and such combustion systems are the topic of this paper. Heat exchangers are periodic structures that consist of arrays of tubes in a cross flow. If sound passes through an array of tubes, it is attenuated due to viscous, thermal and turbulent losses. We aim to utilise this attenuation property of tube arrays to control thermoacoustic instabilities. To this end, we consider an idealised combustion system: the combustion chamber is one-dimensional, the flame is compact and the heat exchanger is a row of narrow sharp-edged rods with rectangular cross-section. Effectively, we treat the heat exchanger as a slit-plate with bias flow.

Slit-plates and, more commonly, orifice plates with a mean flow through the holes (bias flow) are widely used as sound absorbers. A summary of the key contributions to this research topic can be found in the study by

School of Chemical and Physical Sciences, Keele University, Staffordshire, UK

**Corresponding author:**
Maria A Heckl, Keele University, Staffordshire ST5 5BG, UK.
Email: m.a.heckl@keele.ac.uk

Munjal.[2] Generic applications are presented by Davies.[3] The sound absorption of a perforated plate with bias flow can be enhanced greatly by a cavity backing.[4–6]

The idea that a cavity-backed perforated plate can be used in a combustion system to control thermocoustic instabilities was first realised experimentally by Tran et al.[7,8] They implemented a cavity-backed perforated plate at the upstream end of a swirl burner and achieved control by suitable choice of cavity length. Tran's work was continued by Scarpato et al.[9,10] who investigated the role of the Strouhal number on the absorption mechanism of the cavity-backed perforated plate.

A model corresponding to Tran's setup was developed by Heckl and Kosztin,[11] who predicted that control can be achieved for a wide range of cavity lengths. They modelled the flame dynamics by a generic time-lag law and also examined the effectiveness of the control for different time-lags.

Much is known about the damping mechanism of perforated plates with bias flow. When a sound wave hits such a plate, hydrodynamic effects come into play which affect the reflection, transmission and damping of the sound wave. A physically intuitive and experimentally validated model has been developed by Hofmans et al.[12] and Durrieu et al.[13] for a single orifice (both circular and slit-shaped). Their work provides physical insight, which will be valuable for understanding the results in our paper. Below is a summary of their relevant findings.

At the orifice, a free jet is formed by flow separation. The cross-sectional area of the jet is smaller than that of the orifice (vena contracta). One can imagine the orifice as partially blocked by this hydrodynamic effect. Downstream of the orifice, the jet becomes unstable; vortices form and are swept downstream.

The blockage has a strong effect on the acoustic reflection and transmission. The magnitude of the reflection coefficient increases with Mach number, while its phase remains zero. Thus, the orifice behaves like a partially reflective rigid wall. The vortex generation is responsible for the sound absorption, as initially proposed theoretically by Howe.[14] The absorption first increases with Mach number, then reaches a maximum and decreases for higher Mach numbers.

The acoustic behaviour of a perforated plate can be manipulated in a big way by backing it with a cavity. The cavity acts like an acoustic resonator, and as such, it can amplify or damp acoustic waves that enter it. The combination of a perforated plate with bias flow and a backing cavity has been found to become anechoic for certain frequencies and flow Mach numbers.[4,5,6]

For our purpose of describing a heat exchanger as a perforated plate, we are particularly interested in plates with slit-shaped perforations. A comprehensive analytical model for such plates (with and without cavity backing) was produced by Dowling and Hughes.[15] They used the Kutta condition to derive expressions for the reflection and transmission coefficient of the slit-plate. The key parameters in their model are Strouhal number, bias flow Mach number, open area ratio and cavity length.

In this paper, we present a model for an idealised combustion system, which consists of a one-dimensional tube with a compact flame and a jump in mean temperature across the flame or heat source. The upstream end of the tube is open, and the downstream end is formed by a slit-plate, a certain distance upstream of the tube end, which may be open or closed. Surendran and Heckl[16] have already developed a theoretical model for such a combustion system and have shown that the slit-plate with bias flow is an effective method to passively control thermoacoustic instabilities. The present study extends this work in the following ways:

- Instead of the basic $n-\tau$ law, we use an extended (and more versatile) time-lag law to describe the heat source.
- We included a temperature jump at the heat source, rather than assuming a uniform temperature throughout the tube. This assumption of a temperature jump makes the combustor more realistic and close to real situations.
- We examined a wider range of boundary conditions at the downstream tube end.

We begin our analysis with the description of the combustion system and its associated modelling aspects in Section 2. In Section 3, we look at the influence of system parameters on the acoustic properties of the slit-plate and then proceed to the stability predictions (Section 4) for various system parameters, using an eigenvalue method.

## 2 Description of model

The combustion system studied is as shown in Figure 1. It consists of a quarter-wave resonator, open at the

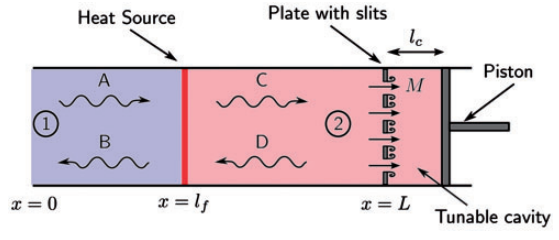


**Figure 1.** Schematic of the combustion system.

upstream end ($x = 0$) and having a reflection coefficient $R_0 = -1$. The heat source is located at a distance $l_f$ from the upstream end, dividing the resonator into two regions: a cold upstream region (Region 1) and a hot downstream region (Region 2). The speeds of sound ($c_{1,2}$) and mean temperatures ($T_{1,2}$) are uniform in both regions. The slit-plate simulating the heat exchanger is located at $x = L$. The slit-plate has a bias flow through the gaps, denoted by its Mach number, $M$. The downstream end of the resonator may be open or closed. In the case of closed end, the downstream extremity is equipped with a rigid piston, enabling us to vary the distance between the slit-plate and the piston. In any case, the distance between the slit-plate and the downstream end is referred to as the cavity length ($l_c$).

## 2.1 Acoustic field

The acoustic field within the combustor is modelled as one-dimensional acoustic waves propagating perpendicular to the rods (normal incidence), as shown in Figure 1. For the present study, we ignore the heat transfer between the rods and the surrounding fluid, i.e., air. The acoustic pressure and velocity fields inside the resonator are,

Region 1 (cold):

$$\hat{p}_1(x) = Ae^{ik_1(x-l_f)} + Be^{-ik_1(x-l_f)} \quad 0 < x < l_f \tag{1}$$

$$\hat{u}_1(x) = \frac{1}{\rho_1 c_1}\left\{Ae^{ik_1(x-l_f)} - Be^{-ik_1(x-l_f)}\right\} \quad 0 < x < l_f \tag{2}$$

Region 2 (hot):

$$\hat{p}_2(x) = Ce^{ik_2(x-l_f)} + De^{-ik_2(x-l_f)} \quad l_f < x < L \tag{3}$$

$$\hat{u}_2(x) = \frac{1}{\rho_2 c_2}\left\{Ce^{ik_2(x-l_f)} - De^{-ik_2(x-l_f)}\right\} \quad l_f < x < L \tag{4}$$

where $\hat{p}$ and $\hat{u}$ are the acoustic pressure and acoustic velocity, respectively (the $\hat{}$ indicates that they are frequency-domain quantities), and $A, B, C$ and $D$ are the pressure amplitudes to be determined. The subscripts 1 and 2 indicate the cold and hot regions respectively within the resonator, and $k_{1,2} = \omega/c_{1,2}$ is the wave number. The factor of $e^{-i\omega t}$ is omitted throughout the analysis.

## 2.2 Generic heat release law

The heat source is assumed to be compact, planar and confined to an infinitesimally thin region at $x = l_f$. For the heat release rate ($\hat{Q}$), we have adopted the generic heat release law by Heckl and Kosztin,[11] where the heat release rate depends on both the instantaneous velocity fluctuations $u(t)$ as well as the time-lagged velocity fluctuations $u(t-\tau)$ at the location $l_f$. It is given by

$$\hat{Q}(\omega) = \alpha\left[n_1\hat{u}(l_f)e^{i\omega\tau} - n_0\hat{u}(l_f)\right] \tag{5}$$

or using Equation (2), by

$$\hat{Q}(\omega) = \frac{\alpha(A-B)}{\rho_1 c_1}\left[n_1 e^{i\omega\tau} - n_0\right] \tag{6}$$

where $\alpha$ is a factor relating the local and global heat release rates, and $n_1$ and $n_0$ are non-dimensional coefficients called coupling coefficients.

## 2.3 Cavity backed slit-plate

The heat exchanger is modelled as an array of thin rods, spaced a distance $d$ apart and having rectangular cross-sections (Figure 2). Therefore, we can treat this array as a plate with slits of width $2s$. A pressure difference across the slit-plate creates a bias flow of Mach number $M$ through the slits, causing vortex shedding. In the model by Dowling and Hughes,[15] the transmission and reflection coefficients of a slit-plate with bias flow were derived as

$$T_{sp} = \rho\omega\dot{V}/(kd) \tag{7}$$

$$R_{sp} = 1 - \rho\omega\dot{V}/(kd) \tag{8}$$

with

$$\frac{\rho\omega\dot{V}}{kd} = \frac{i\pi\nu/(2\kappa sM)}{i\pi\nu/(2\kappa sM) - \ln(\pi\nu) + \ln 2/\Phi} \tag{9}$$

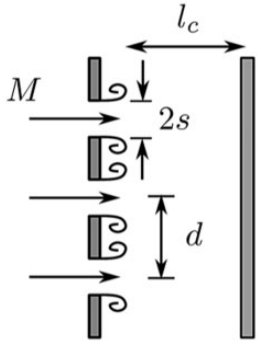


**Figure 2.** Geometry of the slit-plate.

and

$$\Phi = 1 - \frac{1}{\kappa s \ln 2} \times \left\{ \frac{\pi I_0(\kappa s) e^{-\kappa s} + 2i \sinh(\kappa s) K_0(\kappa s)}{\pi e^{-\kappa s}\left[I_1(\kappa s) + \frac{I_0(\kappa s)}{\kappa s \ln 2}\right] + 2i \sinh(\kappa s)\left[\frac{K_0(\kappa s)}{\kappa s \ln 2} - K_1(\kappa s)\right]} \right\} \tag{10}$$

The subscript $sp$ refers to slit-plate and $\dot{V}$ is the perturbation volume flux through the slit. $\nu = 2s/d$ is the open area ratio, $\kappa s = \omega s/U$ is the Strouhal number, $U$ is the bias flow velocity and $I_m$ and $K_m$ are the modified Bessel functions of order $m$. Equations (7)–(10) are valid for $s/d \ll 1$ and $d \ll \lambda$, where $\lambda$ is the wavelength of the incident wave. Further details can be found in the study by Dowling and Hughes.[15] The tube end backing the plate is at a distance $l_c$ from the slit-plate. The effective reflection coefficient, $R_L$, of the cavity-backed slit-plate is given by Surendran and Heckl[16]

$$R_L = R_{sp} + \frac{R_p T_{sp}^2 e^{2ik_2 l_c}}{1 - R_p R_{sp} e^{2ik_2 l_c}} \tag{11}$$

where $R_p$ is the reflection coefficient at the downstream end of the tube. $R_p = 1$, if the end is closed and $R_p = -1$, if it is open.

## 3 Acoustic properties of the cavity-backed slit-plate

We describe the acoustic energy loss at the slit-plate by the absorption coefficient $\Delta_{sp}$, given by

$$\Delta_{sp} = 1 - |T_{sp}|^2 - |R_{sp}|^2 \tag{12}$$

In analogy with this, we write the absorption coefficient of the slit-plate with cavity backing as

$$\Delta_L = 1 - |R_L|^2 \tag{13}$$

$\Delta_{sp}$ and $\Delta_L$ are a measure of the acoustic energy (relative to the incident energy) that is dissipated.

From equations (7)–(13), we can observe that these coefficients depend on the following parameters: bias flow Mach number ($M$), frequency of the wave ($\omega$), cavity length ($l_c$) and open area ratio ($\nu$). We investigate the influence of these parameters in the following four sections, both for the slit-plate in isolation and for the cavity-backed slit-plate.

### 3.1 Influence of Mach number

Figure 3 shows the reflection coefficient (magnitude and phase) and absorption coefficient for a slit-plate in isolation (Figure 3(a), (b), (c)) and for a cavity-backed slit-plate (Figure 3(d), (e), (f)), as function of Mach number for three fixed frequency values: $f = 60$, 120 and 170 Hz. The open area ratio in these figures is 0.1 and the cavity length is 0.5 m.

We observe from Figure 3(a) and (b) that the slit-plate behaves like a partially reflective solid wall ($|R_{sp}| < 1$, $\measuredangle R_{sp} = 0$). As the Mach number increases, the reflectivity increases, while the phase remains zero. This effect has been observed before.[12,13] It is a consequence of the vena contracta effect and boundary layer associated with the bias flow, which increasingly blocks the slits as $M$ increases. Figure 3(c) shows the absorption coefficient $\Delta_{sp}$: it increases initially with $M$ and reaches a maximum of 0.5. The absorption is due to

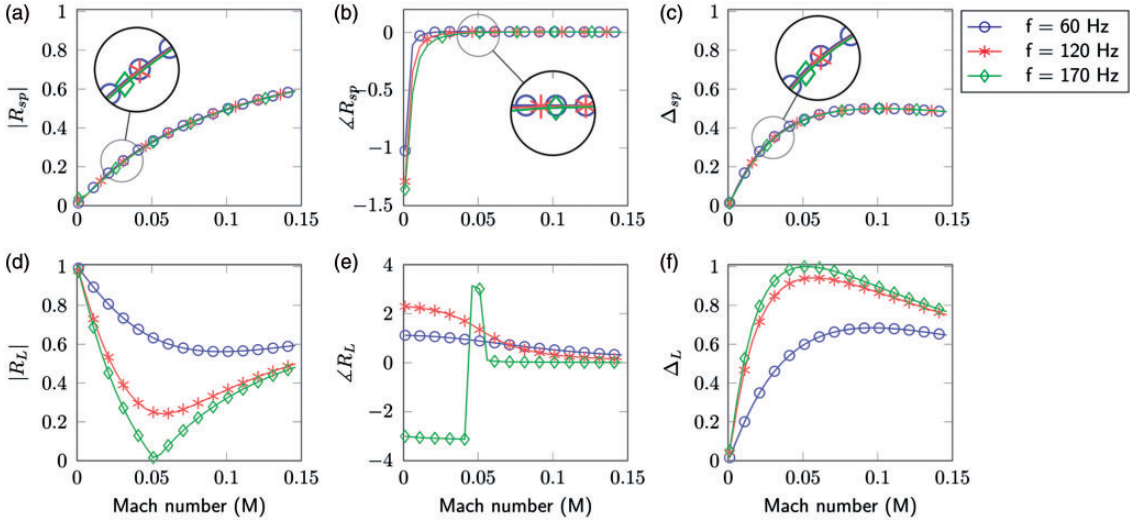


**Figure 3.** Reflection coefficient and absorption coefficient of slit-plate ((a)–(c)) and cavity-backed slit-plate ((d)–(f)) as a function of Mach number, for fixed frequency values and $\nu = 0.1$. For (d)–(f), $l_c = 0.5$ m.

vortices being generated at the downstream slit edges and swept away by the mean flow.[12,13] The reflection and absorption coefficients are weakly dependent on frequency. The zoomed-in plots show this weak dependence on frequency.

The results for the cavity-backed slit-plate are quite different. There is now a pronounced dependence on frequency (see Figure 3(d), (e), (f)). The cavity is an acoustic resonator, which acts like a tube with two closed ends (one of them partially reflective). For the case shown here ($l_c = 0.5$ m), it has an anti-resonance (i.e. a quarter wavelength in the cavity) at the frequency 170 Hz. At this frequency, the reflection coefficient $R_L$ varies widely. It reaches values close to zero for Mach numbers around 0.05, and its phase jumps from $-\pi$ to 0. At this point, the absorption coefficient becomes 1, and the cavity-backed slit-plate behaves like an anechoic end.[15]

### 3.2 Influence of frequency

The influence of frequency on the reflection and absorption coefficients of both slit-plate and cavity-backed slit-plate is shown in Figure 4. The open area ratio is 0.1 and the cavity length is 0.5 m. The slit-plate on its own behaves largely independently of frequency, while the cavity-backed slit-plate shows a strong dependence. As in the previous section, we observe anechoic behaviour for frequencies near 170 Hz at $M = 0.05$. The behaviour is near-anechoic for a substantial range around this frequency: $|R_L| < 0.2$ in the range between 130 Hz and 200 Hz.

### 3.3 Influence of cavity length

Since the anechoic behaviour of the cavity-backed slit-plate is associated with the anti-resonance in the cavity, it is expected that the cavity length has a strong influence. This is indeed the case as can be seen from Figure 5(a), (b) and (c). The frequency values shown are $f = 60$, 120 and 170 Hz, the Mach number is 0.05 and the open area ratio is 0.1. At $l_c = 0$, the slit-plate and the backing wall coincide, effectively forming a rigid wall with complete reflection ($|R_L| = 1$) and no absorption ($\Delta_L = 0$). As $l_c$ increases, $|R_L|$ decreases from 1, attains a minimum and then increases to 1 (Figure 5(a)). At this second maximum, $l_c$ is equal to half the wavelength, and the cavity is at resonance. This alternating behaviour of decreasing and increasing $|R_L|$ continues with increasing $l_c$. At the same time, $\Delta_L$ also alternates, reaching maxima of 1 where $|R_L|$ has minima.

Again, the range where near-anechoic behaviour prevails is quite large: for example, for $f = 120$ Hz, $|R_L| < 0.2$ in the $l_c$ range between 0.6 m and 0.9 m.

### 3.4 Influence of open area ratio

The open area ratio $\nu = 2s/d$ is a measure for the transparency of the slit-plate. Hence, as $\nu$ increases, we expect the slit-plate on its own to become acoustically less reflective and less absorbing. Figure 6(a) and (c) confirms this (for the frequency 170 Hz). The Mach number dependence is also shown in Figure 6. We observe that the phase of $R_{sp}$ is strongly affected by it (see Figure 6(b)): for low $M$ ($M = 0.001$), $\measuredangle R_{sp} = -\pi$, while for higher $M$ ($M = 0.005$, 0.1), $\measuredangle R_{sp} = 0$. This

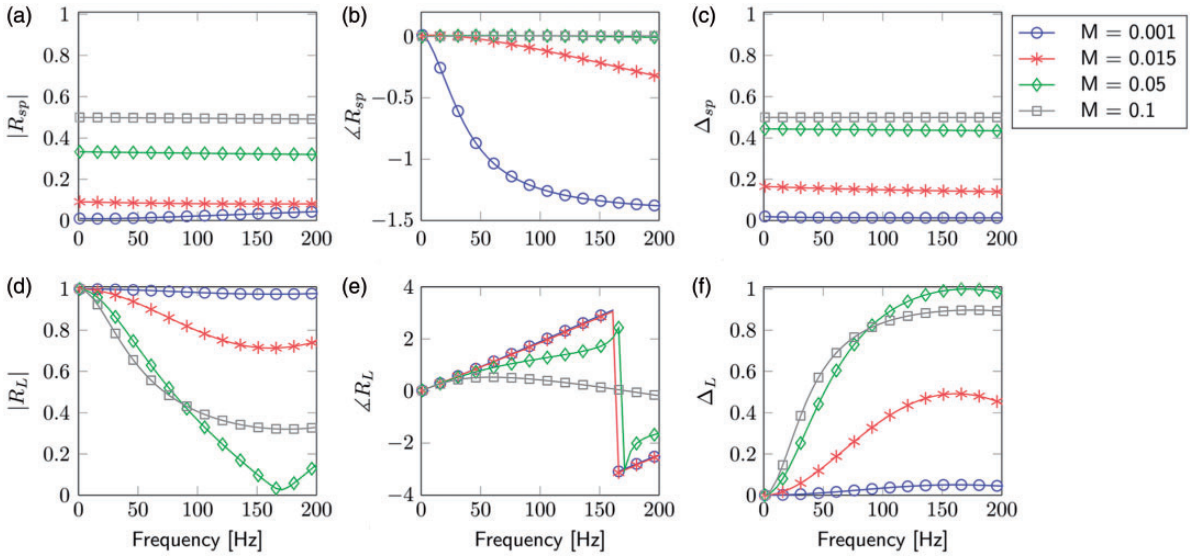


**Figure 4.** Reflection coefficient and absorption coefficient of slit-plate ((a)–(c)) and cavity-backed slit-plate ((d)–(f)) as a function of frequency, for fixed Mach numbers and $\nu = 0.1$. For (d)–(f), $l_c = 0.5$ m.

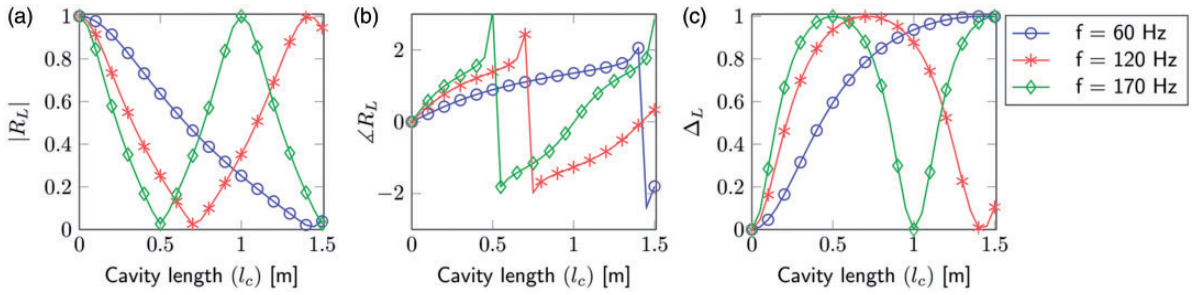


**Figure 5.** Reflection coefficient ((a)–(b)) and absorption coefficient ((c)) of cavity-backed slit-plate, as a function of cavity length, for fixed frequencies, $M = 0.05$ and $\nu = 0.1$.

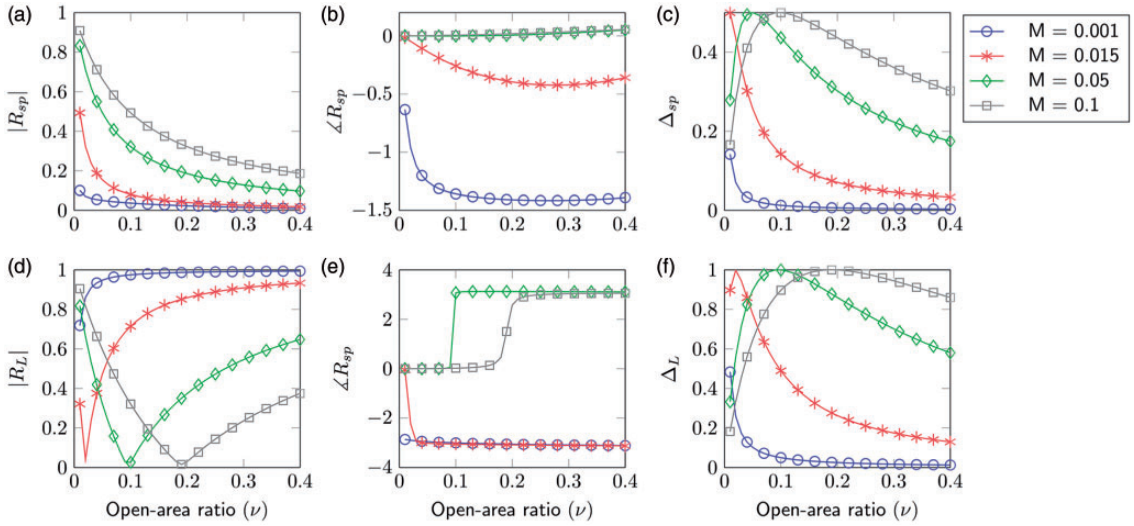


**Figure 6.** Reflection coefficient and absorption coefficient of slit-plate ((a)–(c)) and cavity-backed slit-plate ((d)–(f)) as a function of open area ratio, for fixed Mach numbers and $f = 170$ Hz. For (d)–(f), $l_c = 0.5$ m.

can again be explained by the hydrodynamic blockage effects (vena contracta and boundary layer) mentioned in Section 3.1. As a result, the slit-plate in isolation behaves like an increasingly reflective rigid wall as the Mach number increases; also its ability to absorb weakens as $\nu$ increases because less vortex shedding occurs.

The consequences for the cavity-backed slit-plate are shown in Figure 6(d), (e), (f), again for the case $f = 170$ Hz and $l_c = 0.5$ m. Except for the lowest Mach number ($M = 0.001$), $|R_L|$ decreases for small $\nu$ values, reaches a minimum and then steadily increases. At the minimum, $\measuredangle R_L$ jumps from 0 to $\pm\pi$, and $\Delta_L$ reaches the optimal value of 1. The width of the minimum of $|R_L|$ and maximum of $\Delta_L$ is again conveniently wide, as is the case for the parameters examined in the previous three sections.

### 3.5 Influence of open-end cavity

We also considered the case of a cavity bounded by an open end (rather than a closed end) at $x = L + l_c$ and investigated the dependence on the parameters $M$, $f$, $l_c$ and $\nu$. The results (not shown) are very similar: $|R_L|$ has a minimum when the cavity is at anti-resonance; this now happens when the cavity length is equal to half a wavelength. The optimal values for $M$, $f$, $l_c$ and $\nu$ change, but $|R_L|$ is still close to 0 and $\Delta_L$ is still close to 1 in a large parameter range.

In summary, for a given $f$, the absorption coefficient of a cavity-backed slit-plate can be maximised if we choose the appropriate $l_c$, $\nu$ and $M$. In the case of a combustor with an unstable mode, the frequency of the unstable mode is known. Therefore, given a fixed slit-plate dimension, we aim to stabilise the combustor by choosing the appropriate bias flow Mach number, $M$, and cavity length, $l_c$.

## 4 Stability predictions

For stability predictions, we make use of the eigenvalue method,[17] which is instrumental in obtaining the growth rates of different modes in the system. In the

present work, we restrict ourselves to the first and second modes of the combustor.

### 4.1 Boundary and jump conditions

The unknowns in our system are the four pressure amplitudes $A$, $B$, $C$ and $D$. Therefore, we need four homogeneous equations, obtained from the following boundary and jump conditions.

At $x = 0$ :

$$Ae^{-ik_1 l_f} = R_0 Be^{ik_1 l_f} \tag{14}$$

At $x = L$ :

$$De^{-ik_2(L-l_f)} = R_L Ce^{ik_2(L-l_f)} \tag{15}$$

$R_0$ and $R_L$ are the reflection coefficients at $x = 0$ and $x = L$, respectively.

Across the heat source ($x = l_f$), we assume continuity of pressure,

$$A + B = C + D \tag{16}$$

and a velocity jump generated by the heat source[18]

$$-\frac{(A-B)}{\rho_1 c_1} + \frac{(C-D)}{\rho_2 c_2} = \frac{(\gamma-1)}{\rho_1 c_1^2 S}\hat{Q}(l_f) \tag{17}$$

where $S$ is the cross-sectional area of the duct and $\gamma$ is the ratio of the specific heat capacities.

### 4.2 Eigenfrequencies and growth rates

Equations (14)–(17) can be rearranged in matrix form to yield:

$$[Y(\Omega)]\begin{bmatrix} A \\ B \\ C \\ D \end{bmatrix} = \begin{bmatrix} 0 \\ 0 \\ 0 \\ 0 \end{bmatrix} \tag{18}$$

with

$$Y(\Omega) = \begin{bmatrix} e^{-i\frac{\Omega}{c_1}l_f} & -R_0 e^{i\frac{\Omega}{c_1}l_f} & 0 & 0 \\ 0 & 0 & R_L e^{i\frac{\Omega}{c_2}(L-l_f)} & -e^{-i\frac{\Omega}{c_2}(L-l_f)} \\ 1 & 1 & -1 & -1 \\ \left(-1-\beta_1 e^{i\Omega\tau}+\beta_0\right) & \left(1+\beta_1 e^{i\Omega\tau}-\beta_0\right) & \zeta & -\zeta \end{bmatrix} \tag{19}$$

where $\beta_{0,1} = \left(\alpha n_{0,1}(\gamma-1)\right)/\left(S\rho_1 c_1^2\right)$ is a quantity proportional to the coupling coefficients and $\zeta = (\rho_1 c_1)/(\rho_2 c_2)$ is the ratio of the specific impedances.

Solution of the characteristic equation, $\det Y(\Omega) = 0$, using the Newton Raphson or bisection method, gives us the eigenfrequencies of the system. The solution $\Omega_m = \omega_m + i\delta_m$ is a complex quantity where $\omega_m$ denotes the natural frequency of the mode $m$ and $\delta_m$ its growth rate. Positive $\delta_m$ indicates instability and negative $\delta_m$ indicates stability.

### 4.3 Stability maps – closed end

From equation (19), one can infer that the parameters which affect the stability of the combustor are: the properties of the medium inside the duct ($\rho_{1,2}$, $c_{1,2}$, $T_{1,2}$), the duct length ($L$), the location of the heat source ($l_f$), the reflection coefficients at the boundaries ($R_0$ and $R_L$), the time-lag ($\tau$) and the heat release rate law properties ($\alpha$ and $n_{0,1}$). In addition to these parameters, cavity length ($l_c$), slit-plate dimensions ($d$ and $v$) and bias flow Mach number ($M$) have an indirect influence through $R_L$. Here, we consider the influence of the following three parameters: cavity length, heat source location and bias flow Mach number.

The stability maps are constructed in the cavity length ($l_c$) – heat source location ($l_f$) plane, where the *grey* regions indicate instability and the *white* regions indicate stability. Stability of any mode is determined from the sign of its growth rate, as mentioned in the previous section. In our study, we look at the stability of the first two modes of the system. The cold region is assumed to be at room temperature ($T_1 = 288\,\mathrm{K}$) and the hot region is assumed to be at $T_2 = 1288\,\mathrm{K}$. The duct length $L$ is assumed to be 1 m, duct cross-section $S$ is assumed to be $0.05 \times 0.05\ \mathrm{m}^2$ and the heat release rate law properties are taken as constants: $\alpha = 120$ kg m/s$^2$, $n_1 = 1.2$, $n_0 = 0.2$ and $\tau = 0.15 \times 10^{-3}$ s. Table 1 shows the range of the conservative estimates of the time periods for the first and second eigenmodes. We can observe that the time-lag chosen in our analysis is much smaller than the fundamental periods encountered in the stability analysis. The complete list of system parameters used in the forthcoming analysis is given in Table 2.

Firstly, we construct the stability map for mode 1 of a quarter-wave resonator containing only a heat source and no slit-plate, for two temperature distributions: $T_1 = T_2 = 288\,\mathrm{K}$ (Figure 7 (a)) and $T_1 = 288\,\mathrm{K}$, $T_2 = 1288\mathrm{K}$ (Figure 7(b)). We observe from the plots that the system is unstable for the range of values of $l_c$ and $l_f$ considered. This behaviour can be explained in terms of the mode shape of the wave within the resonator. In the absence of the slit-plate, an increase in cavity length ($l_c$) effectively adds to the duct length, $L$. The total length of the resonator will now be $(L + l_c)$. The first mode shape of the quarter-wave resonator will be, as the name suggests, a quarter wave with a node at $x = 0$ and a maximum at $x = (L + l_c)$. From the Rayleigh criterion, we can conclude this instability behaviour of the first mode of the resonator, regardless of the cavity length and heat source location considered.

**Table 1.** Range of time periods of the eigenfrequencies in the stability maps.

| Mode | Temperature distribution | Time period range |
|---|---|---|
| 1 | $T_1 = 288$ K, $T_2 = 1288$ K | $[5.6 \ldots 16.6] \times 10^{-3}$ s |
| 2 | $T_1 = 288$ K, $T_2 = 1288$ K | $[1.4 \ldots 5.2] \times 10^{-3}$ s |

**Table 2.** List of system parameters used.

| Parameter | Notation | Value |
|---|---|---|
| Temperature [K] | $\boldsymbol{T_1}$ | 288 |
| | $\boldsymbol{T_2}$ | 1288 |
| Density [kg/m$^3$] | $\rho_1$ | 1.2 |
| | $\rho_2$ | 0.268 |
| Speed of sound [m/s] | $\boldsymbol{c_1}$ | 341 |
| | $\boldsymbol{c_2}$ | 721.5 |
| Duct length [m] | $L$ | 1 |
| Cross-sectional area [m$^2$] | $\boldsymbol{S}$ | 0.0025 |
| Cavity length [m] | $\boldsymbol{l_c}$ | $[0 \cdots \boldsymbol{L}/2]$ |
| Heat source location [m] | $\boldsymbol{l_f}$ | $[0 \cdots \boldsymbol{L}]$ |
| Time-lag law parameters | $\alpha$ [kg m/s$^2$] | 120 |
| | $\boldsymbol{n_1}$ | 1.2 |
| | $\boldsymbol{n_0}$ | 0.2 |
| | $\tau$ [s] | $0.15 \times 10^{-3}$ |
| Slit-plate | $\boldsymbol{d}$ [m] | 0.02 |
| | $\nu$ | 0.1 |

Next, we introduce a slit-plate with bias flow into the system. The slit dimensions are $d = 0.02\,\mathrm{m}$ and $\nu = 0.1$. The present study is an extension to the work by Surendran and Heckl,[19] where they investigated the effect of the bias flow Mach number $M$ and cavity length on the stability of a quarter-wave resonator with a heat source obeying the simple $n - \tau$ law. They observed that the stability of the first mode increased with increasing $M$. Figure 8 shows the stability maps obtained for the current resonator configuration with uniform temperature distribution and generic heat release law. In this study also, the stability maps exhibit trends similar to those reported by Surendran and Heckl.[19] At very low $M$, the unstable region is larger compared to the stable region (Figure 8(a)). As we increase $M$, the stable region increases (Figure 8(b) and (c)). We also get a range of $l_c$ values where the resonator is stable, irrespective of the location of the heat source.

The influence of $l_c$ and $M$ on the stability of the combustor can be explained through the contour plot of $\omega_1$, the real part of the complex eigenfrequency $\Omega_1$, as shown in Figure 9. The contours vary in the range ~55–85 Hz, and correspond to mode 1 of the combustor with $T_1 = T_2 = 288\,\mathrm{K}$. The eigenfrequencies decrease with increasing $l_c$ and from Figure 5(c), we can conclude that for a given bias flow $M$, an acoustic wave of 55 Hz with $\boldsymbol{l_c} = 0.5\,\mathrm{m}$ has higher absorption

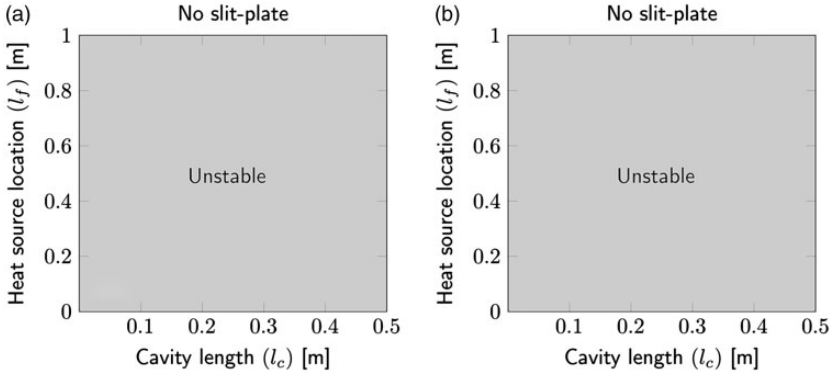


**Figure 7.** Stability map for mode 1 without slit-plate and bias flow with (a) $T_1 = T_2 = 288$ K and (b) $T_1 = 288$ K and $T_2 = 1288$ K.

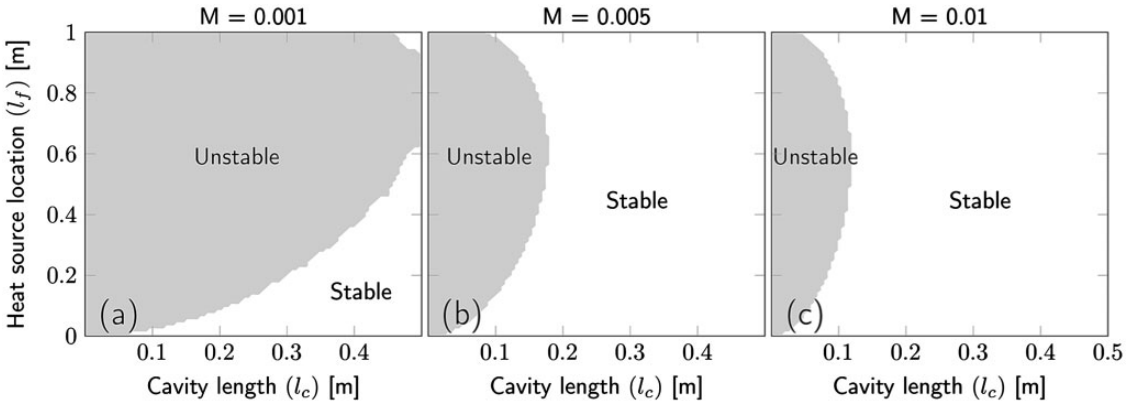


**Figure 8.** Stability maps for mode I and different Mach numbers (a) $M = 0.001$, (b) $M = 0.005$ and (c) $M = 0.01$, for a combustor with $T_1 = T_2 = 288$K.

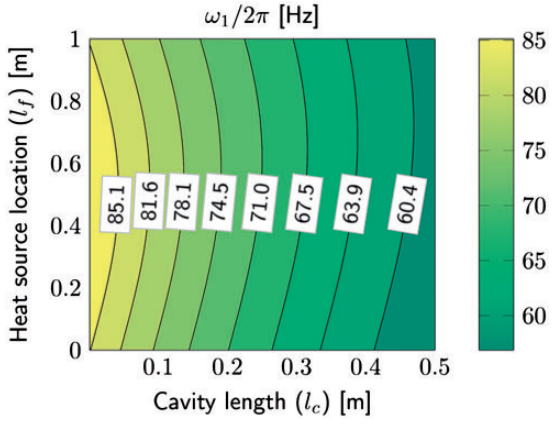


**Figure 9.** Eigenfrequency ($\omega_1/2\pi$) (Hz) contour for mode I of the combustor with $T_1 = T_2 = 288$ K.

than a wave of 80 Hz with $l_c = 0.1$ m. The influence of bias flow $M$ is shown in Figure 3(f). For a given frequency and $l_c$, the absorption increases with increasing $M$. Combining these effects, we can explain the stability maps shown in Figure 8. The combustor starts to stabilise for higher $l_c$, and the stable regions grow as we increase the bias flow $M$.

As a step further to our study, we also incorporated a temperature jump across the heat source ($T_1 = 288$ K and $T_2 = 1288$ K). The stability maps, again constructed in the $l_f$ –$l_c$ plane for three Mach numbers: $M = 0.001$, 0.005 and 0.01, are given in Figure 10. Comparison of Figure 10 and Figure 8 shows that having a hot region or temperature nonuniformity within the combustor tends to de-stabilise it, i.e., the unstable regions are larger. But in this case also, we can extend the stable regions of the system by increasing $M$. Hence, it is still possible to find a cavity length and Mach number that stabilises the combustion system.

Similar stability maps can also be constructed for the second mode of the resonator. Here also, we start with the no slit-plate case. Figure 11(a) and (b) shows the stability maps for the second mode when we have uniform and nonuniform temperature distribution, respectively. The stability maps are as expected. In the second mode, we have three-quarters of a wave within the combustor and as the heat source changes its position from the inlet towards the slit-plate, we get constructive and destructive interaction between the heat release rate fluctuations and the acoustic pressure fluctuations leading to alternating stable and unstable regions. In Figure 11(a), the small unstable region near $l_c = 0.5$ m for $l_f = [0.5 \cdots 1]$ m is caused by non-convergence of the numerical method used. Ideally, this region should also be stable.

Now, we introduce the slit-plate with the bias flow. Figure 12 shows the stability maps for mode 2 of the combustor with uniform temperature distribution and Figure 13 shows the stability maps when there is nonuniform temperature distribution. We observe that the unstable regions get fragmented and slowly turn into stable regions as we increase $M$. The effect of Mach number is similar for both the temperature distributions. Again, we are able to find ranges for the Mach number and cavity length that could stabilise the already unstable modes of the combustor. In Figure 12(a) also, the small region near $l_c = 0.5$ m for $l_f = [0 \cdots 1]$ m should have been stable. But this unstable region is caused by non-convergence of the numerical method used.

### 4.4 Stability maps – open end

In this section, we look at the stability maps for the resonator with open ends. The stability maps are again constructed in the cavity length ($l_c$) – heat source location ($l_f$) plane. The properties of the system are the same as those given in the previous section. The cold region is assumed to be at room

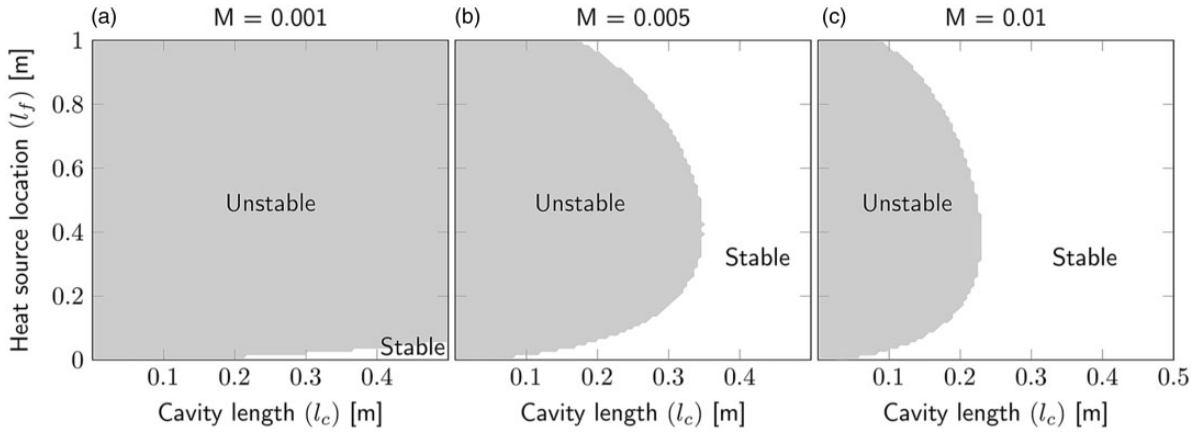


**Figure 10.** Stability maps for mode 1 and different Mach numbers (a) $M = 0.001$, (b) $M = 0.005$ and (c) $M = 0.01$, for a combustor with $T_1 = 288$ K and $T_2 = 1288$ K.

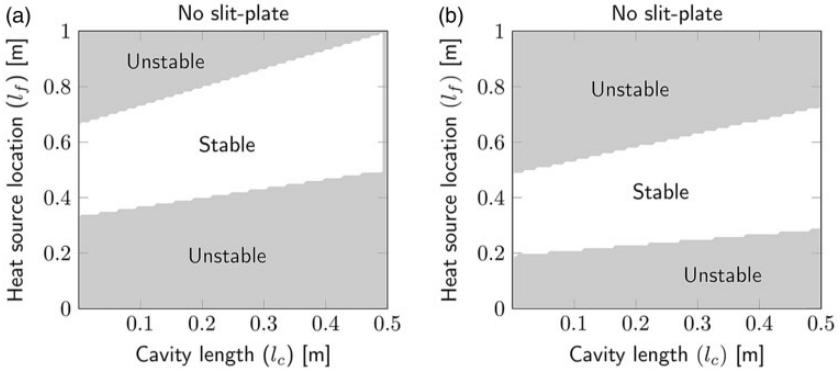


**Figure 11.** Stability map for mode 2, without slit-plate and bias flow with (a) $T_1 = T_2 = 288$ K and (b) $T_1 = 288$ K and $T_2 = 1288$ K.

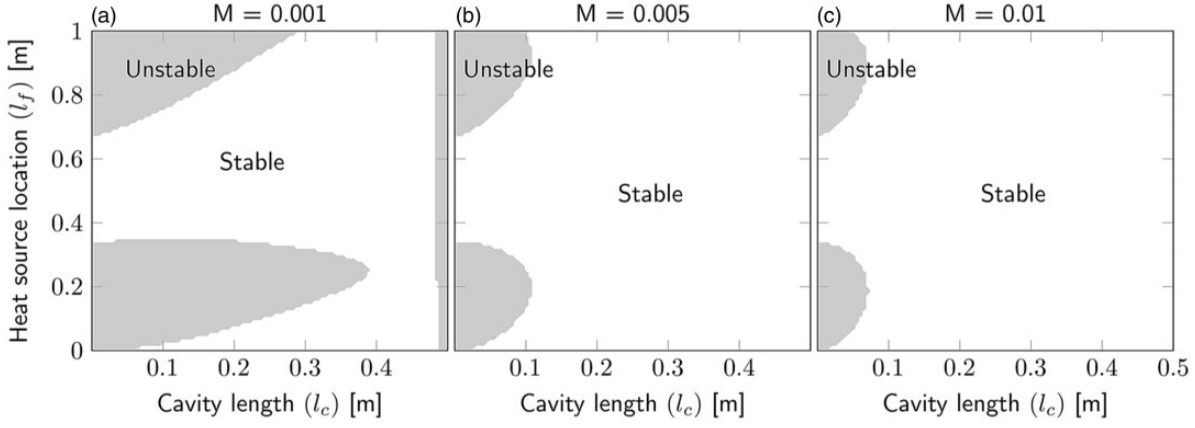


**Figure 12.** Stability maps for mode 2 and different Mach numbers (a) $M = 0.001$, (b) $M = 0.005$ and (c) $M = 0.01$, for a combustor with $T_1 = T_2 = 288$ K.

temperature ($T_1 = 288$ K) and the hot region is assumed to be at $T_2 = 1288$ K. The duct length $L$ is assumed to be 1 m, the duct cross-section $S$ is assumed to be $0.05 \times 0.05$ m$^2$ and the heat release rate law properties are taken as constants: $\alpha = 120$ kg m/s$^2$, $n_1 = 1.2$, $n_0 = 0.2$ and $\tau = 0.15 \times 10^{-3}$ s. Table 3 shows the range of the conservative estimates of the time periods for the first and second eigenmodes. The time-lag

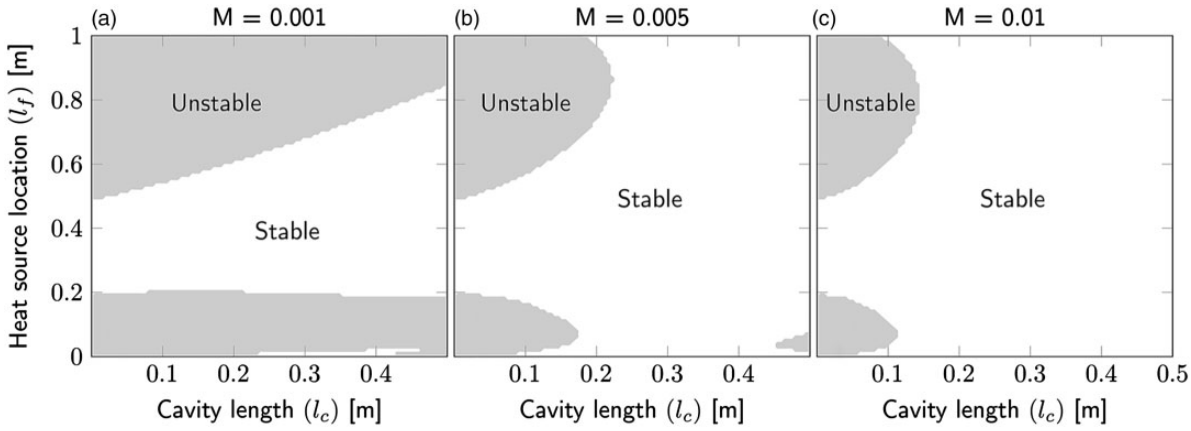


**Figure 13.** Stability maps for mode 2 and different Mach numbers (a) $M = 0.001$, (b) $M = 0.005$ and (c) $M = 0.01$, for a combustor with $T_1 = 288$ K and $T_2 = 1288$ K.

**Table 3.** Range of time periods of the eigenfrequencies in the stability maps.

| Mode | Temperature distribution | Time period range |
|---|---|---|
| 1 | $T_1 = 288\,\text{K}$, $T_2 = 1288\,\text{K}$ | $[2.7 \cdots 6.7] \times 10^{-3}\,\text{s}$ |
| 2 | $T_1 = 288\,\text{K}$, $T_2 = 1288\,\text{K}$ | $[1.3 \cdots 3.5] \times 10^{-3}\,\text{s}$ |

chosen is much smaller than the fundamental periods encountered in the stability analysis.

Like in the previous section, we start with the stability maps for the no slit-plate case. Figure 14 shows the stability maps for mode 1 of the resonator with no slit-plate, for uniform (Figure 14 (a)) and nonuniform (Figure 14 (b)) temperature distributions. The results obtained for the uniform temperature distribution (Figure 14 (a)) show that the resonator is stable when the heat source is placed in the lower half (downstream section) of the resonator. This is because the first mode shape within the resonator is half a wave with nodes at $x = 0$ and $x = (L + l_c)$, and using the Rayleigh criterion, we can deduce that the system will have a stable mode when the heat source is placed in the lower half of the resonator. When there is a temperature jump, we observe that the stable region is larger (Figure 14(b)), and this can be attributed to the frequency shift due to the temperature jump and the changes in the speed of sound. In other words, the presence of the heat source and the consequent temperature jump modifies the mode shape such that we get a constructive interference between acoustic pressure fluctuations and heat release rate fluctuations leading to stable behaviour.

The introduction of slit-plate with bias flow changes the stability behaviour significantly. Figures 15 and 16 show the stability maps for the resonator with uniform and nonuniform temperature distribution, respectively, after the inclusion of the slit-plate with bias flow. The Mach number $M$ increases from plots (a) to (c), and we observe the increased stability of the resonator. Unlike the closed end case, in the open end situation, we get complete stability for higher $M$ values (Figures 15 and 16(b) and (c)).

Finally, stability maps are also constructed for the second mode of the open end resonator. The no slit-plate cases for the two temperature distributions are shown in Figure 17(a) and (b). The alternating unstable and stable bands are due to the mode shape of the pressure wave and its interaction with the heat release rate fluctuations. In the second mode, we have a full wave within the combustor leading to alternating stable and unstable regions.

Figure 18 shows the stability maps for mode 2 of the combustor with uniform temperature distribution and Figure 19 shows the stability maps for the nonuniform temperature distribution. We observe that the unstable regions decrease as we increase $M$. The effect of Mach number is similar for both the temperature distributions. There is a wide range of cavity lengths that could stabilise the unstable mode of the resonator.

## 5 Summary and outlook

We presented a model for an idealised combustor with heat exchanger to predict its stability behaviour. The combustion system consisted of a one-dimensional tube with a compact flame and a mean temperature jump across the heat source. The heat exchanger is modelled as an array of thin sharp-edged rods with rectangular cross-sections. Hence, the heat exchanger was treated as a slit-plate. We also included a bias flow through the slits to enhance the sound absorption characteristic of the slit-plate. Instead of a simple $n - \tau$ law, we have used an extended version of the time-lag law to describe the heat source.

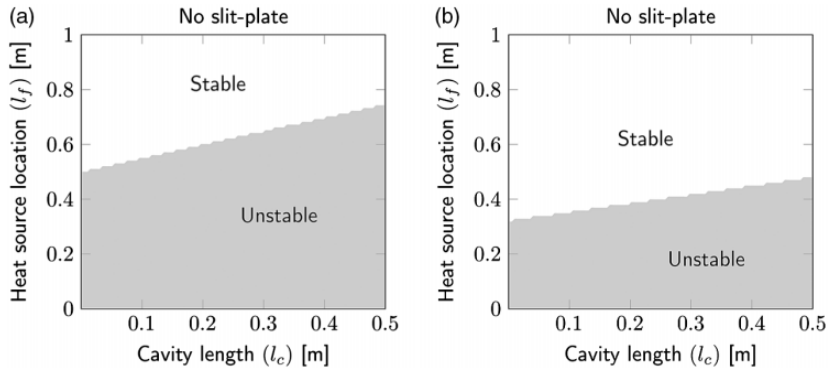


**Figure 14.** Stability map for mode I without slit-plate and bias flow with (a) $T_1 = T_2 = 288$ K and (b) $T_1 = 288$ K and $T_2 = 1288$ K.

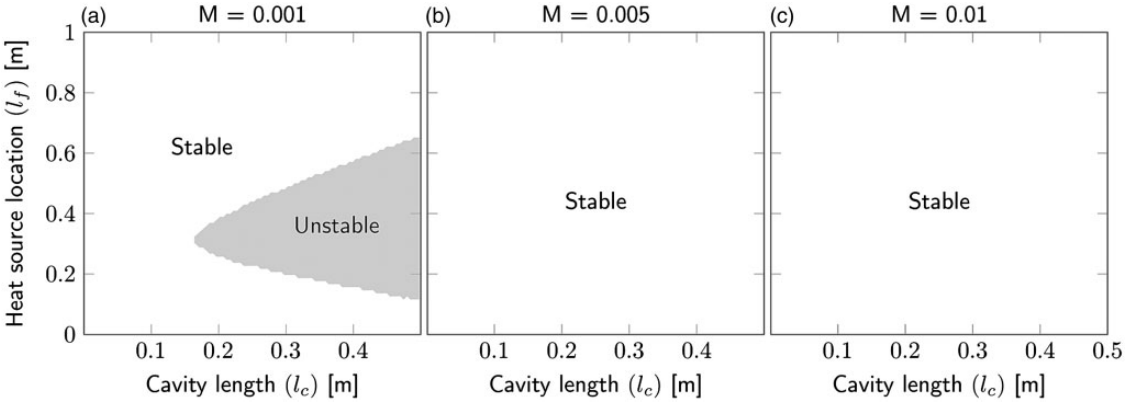


**Figure 15.** Stability maps for mode I and different Mach numbers (a) $M = 0.001$, (b) $M = 0.005$ and (c) $M = 0.01$, for a combustor with $T_1 = T_2 = 288$ K.

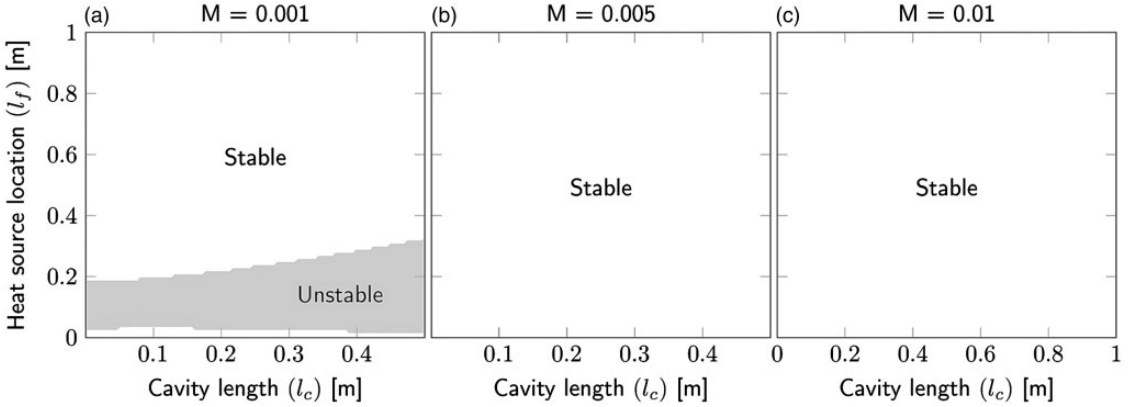


**Figure 16.** Stability maps for mode I and different Mach numbers (a) $M = 0.001$, (b) $M = 0.005$ and (c) $M = 0.01$, for a combustor with $T_1 = 288$ K and $T_2 = 1288$ K.

Our model is applied to the idealised combustion system with tuneable downstream end condition, that is, by varying the aeroacoustic properties of the slit-plate backed by an open end or a rigid end, we can tune the downstream reflection coefficient. Stability maps constructed in the cavity length ($l_c$) – location of heat source ($l_f$) plane yield the following results:

- The unstable mode of a combustor can be controlled passively by a bias-flow slit-plate provided that the

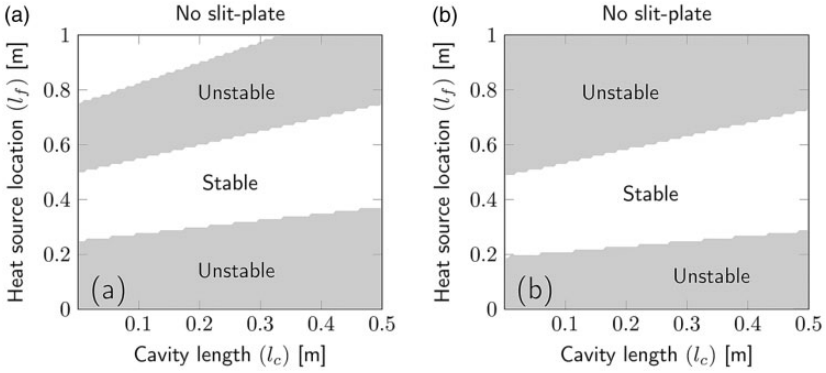


**Figure 17.** Stability map for mode 2 without slit-plate and bias flow with (a) $T_1 = T_2 = 288$ K and (b) $T_1 = 288$ K and $T_2 = 1288$ K.

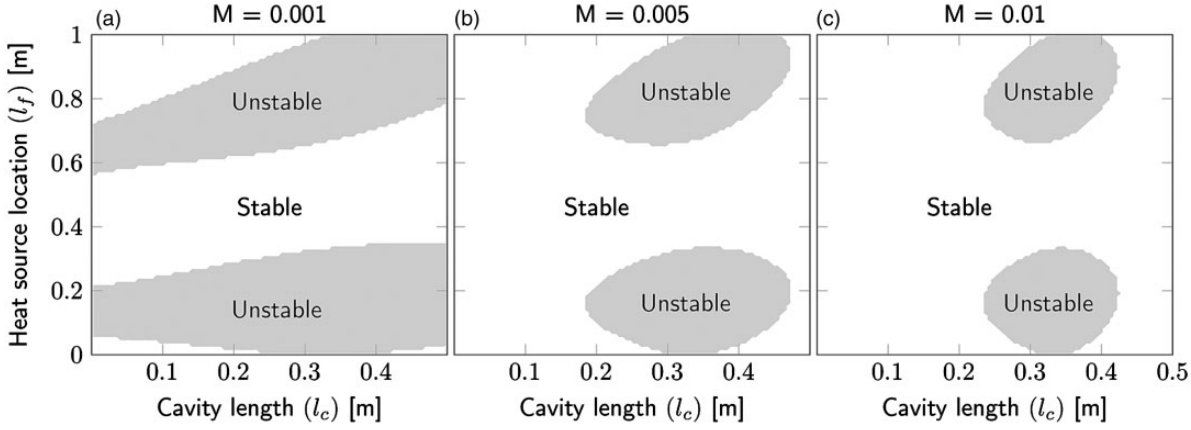


**Figure 18.** Stability maps for mode 2 and different Mach numbers (a) $M = 0.001$, (b) $M = 0.005$ and (c) $M = 0.01$, for a combustor with $T_1 = T_2 = 288$ K.

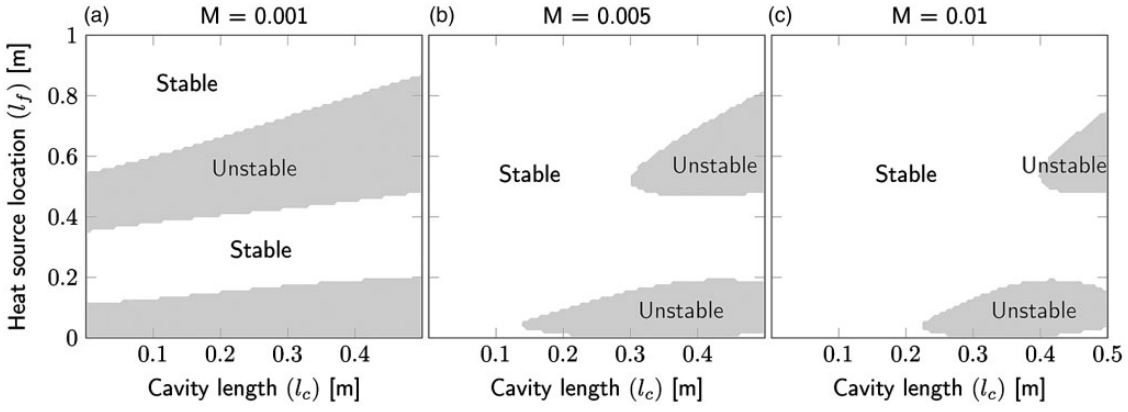


**Figure 19.** Stability maps for mode 2 and different Mach numbers (a) $M = 0.001$, (b) $M = 0.005$ and (c) $M = 0.01$, for a combustor with $T_1 = 288$ K and $T_2 = 1288$ K.

bias flow Mach number and the cavity length are chosen appropriately.

- For a particular unstable mode, an increase of the bias flow Mach number tends to enhance the stability of that mode.
- There is a wide range of cavity lengths, for fixed Mach number, that can be utilised to enhance the stability of the combustor,
- The temperature jump at the flame has a significant effect on the combustor's stability behaviour: it can

be stabilising or destabilising, and it is therefore important to include it in the model.

With our model, we are able to find a broad range of values for the bias flow Mach number and the cavity length that can be used to stabilise the already unstable modes of the combustion system considered. These findings have practical implications for combustion systems like domestic boilers. The need for clean and compact boilers makes it difficult for the inclusion of passive control components like quarter-wave resonators and Helmholtz resonators, that are generally bulky. In such situations, it is a viable alternative to use heat exchangers to control thermoacoustic instabilities.

In a domestic boiler, the heat exchanger is housed within the combustion chamber, along with the flame, and therefore there is no requirement for additional space. Our study shows that there is a wide range of values for $l_c$ (distance between heat exchanger and combustion chamber end) and for $M$ (Mach number of the flow through the gaps between the heat exchanger tubes) that stabilise a previously unstable combustion system. This form of passive instability control improves the design flexibility of domestic boilers, as no additional components are required. It opens the door for new designs of efficient and reliable boilers with reduced pollution of the environment.

## Acknowledgements

The presented work is part of the Marie Curie Initial Training Network Thermo-acoustic and Aero-acoustic Nonlinearities in Green combustors with Orifice structures (TANGO). The authors are also thankful to Prof. Avraham Hirschberg, Technical University of Eindhoven, for the fruitful discussions on the acoustic behaviour of slit-plates in a duct.

## Declaration of Conflicting Interests

The author(s) declared no potential conflicts of interest with respect to the research, authorship, and/or publication of this article.

## Funding

The author(s) disclosed receipt of the following financial support for the research, authorship, and/or publication of this article: We gratefully acknowledge the financial support from the European Commission under call FP7-PEOPLE-ITN-2012.

## References

1. Lieuwen TC and Yang V. *Combustion instabilities in gas turbine engines: operational experience, fundamental mechanisms, and modeling*. Reston, VA: American Institute of Aeronautics and Astronautics, Inc., 2005.
2. Munjal ML. *Acoustics of ducts and mufflers – with application to exhaust and ventilation system design*. New York: John Wiley and Sons Ltd., 1987.
3. Davies POAL. Practical flow duct acoustics. *J Sound Vib* 1988; 124: 91–115.
4. Ronneberger D. Experimentelle Untersuchungen zum akustischen Reflexionsfaktor von unstetigen Querschnittsänderungen in einem luftdurchströmten Rohr [Experimental investigations about the acoustic reflection coefficient of discontinuous changes of cross-section in tubes with air flow]. *Acustica* 1967; 19: 222–235.
5. Bechert DW. Sound absorption caused by vorticity shedding, demonstrated with a jet flow. *J Sound Vib* 1980; 70: 389–405.
6. Hughes IJ and Dowling AP. The absorption of sound by perforated linings. *J Fluid Mech* 1990; 218: 299–335.
7. Tran N, Ducruix S and Schuller T. Damping combustion instabilities with perforates at the premixer inlet of a swirled burner. *Proc Combust Inst* 2009; 32: 2917–2924.
8. Tran N, Ducruix S and Schuller T. Passive control of the inlet acoustic boundary of a swirled burner at high amplitude combustion instabilities. *ASME J Eng Gas Turb Power* 2009; 131: 051502/1–7.
9. Scarpato A, Tran N, Ducruix S, et al. Modeling the damping properties of perforated screens traversed by a bias flow and backed by a cavity at low Strouhal number. *J Sound Vib* 2012; 331: 276–290.
10. Scarpato A, Ducruix S and Schuller T. A comparison of the damping properties of perforated plates backed by a cavity operating at low and high Strouhal numbers. *Comptes Rendus Mécanique* 2013; 341: 161–170.
11. Heckl M and Kosztin B. Analysis and control of an unstable mode in a combustor with tuneable end condition. *Int J Spray Combust Dynam* 2013; 5: 243–272.
12. Hofmans GCJ, Boot RJJ, Durrieu PPJM, et al. Aeroacoustics response of a slit-shaped diaphragm in a pipe at low Helmholtz number, 1: Quasi-steady results. *J Sound Vib* 2001; 244: 35–56.
13. Durrieu P, Hofmans G, Ajello G, et al. Quasisteady aeroacoustic response of orifices. *J Acoust Soc Am* 2001; 110: 1859–1872.
14. Howe MS. On the theory of unsteady high Reynolds number flow through a circular aperture. *Proc Math Phys Eng Sci* 1979; 366: 205–223.
15. Dowling AP and Hughes IJ. Sound absorption by a screen with a regular array of slits. *J Sound Vib* 1992; 156: 387–405.
16. Surendran A and Heckl MA. Analytical study of a Rijke tube with heat exchanger. In: *The 21st international congress on sound and vibration*, Beijing, China, 13–17 July 2014.
17. Heckl MA. *Heat sources in acoustic resonators*. PhD Thesis, Emmanuel College, Cambridge, 1985.
18. Heckl MA. Active control of the noise from a Rijke tube. *J Sound Vib* 1988; 124: 117–133.
19. Surendran A and Heckl MA. Passive instability control by using a heat exchanger as acoustic sink. In: *The 22nd international congress on sound and vibration*, Florence, Italy, 12–16 July 2015.